A Movable-Mass Attitude Stabilization System For Cable-Connected Artificial-g Space Stations

DARA W. CHILDS,* AND THERMAN L. HARDISON†
University of Louisville, Louisville, Ky.

The development of an active, momentum-exchange system to be used for attitude stabilization of a class of cable-connected artificial-g space stations is studied. A system which employs a single movable control mass is examined for the control of a space station which has the physical appearance of two cylinders connected axially by cables. The dynamic model for the space station includes its aggregate rigid body rotation and relative "torsional" rotation between the bodies. A zero torsional stiffness design (one cable) and a maximum torsional stiffness design (eight cables) are examined in various (0, $\frac{1}{4}$, $\frac{1}{2}$, $\frac{3}{4}$, 1) stages of deployment, for selected spin velocities ranging from 4 rpm upwards. A linear, time-invariant, feed-back control system is employed, with gains calculated via a root-specification procedure. The movable mass controller (MMC) provides critical wobble-damping capability for the crew quarters for all configurations and spin velocity. The complete MMC system has a projected Earth weight of approximately 500 lbs. For the fully-deployed space station examined in this study, at the nominal spin-velocity of 4 rpm, the peak-force requirements for the system are on the order of 15 lb for the maximum stiffness design, and 5 lb for the zero stiffness design. The corresponding mechanical power requirements for the system are 6 and 36 w for the zero and maximum stiffness designs, respectively.

Nomenclature

a = $(I_z-I_y)/I_x$
b = $(I_z-I_x)/I_y$
b_1 = $(I_{z1}{}^1-I_{x1}{}^1)/I_y{}^1$
b_2 = $(I_{z2}{}^2-I_{x2}{}^2)/I_y{}^2$
C_1 = distance from the mass center of body 1 to the system mass center
C_2 = distance from the mass center of body 1 to the mass center of body 2
e = $I_y{}^2/I_x$
e_1 = $m_c r_y{}^2/I_x+m_c r_x{}^2/I_y{}^1$
g_2 = $m_c r_y/I_x$
g_1 = $m_c r_x/I_y{}^1$
I_x, I_y, I_z = moment of inertias in the x, y, z system of the space station treated as a rigid body
$I_x{}^1, I_y{}^1, I_z{}^1$ = moment of inertias in the x, y, z system for body 1
$I_x{}^2, I_y{}^2, I_z{}^2$ = principal moment of inertias in the x^2, y^2, z^2 system for body 2
$I_{yz}(0), I_{xz}(0)$ = initial product of inertia disturbances for the space station
k_i = feedback gains
k_t = torsional stiffness coefficient for cable connections
m_c = control mass magnitude
p_1 = undamped crew-quarter wobble frequency
p_2 = undamped torsional natural frequency
p_3 = undamped natural frequency of the stabilized control mass
P^2 = $(I_y{}^1+I_y{}^2)k_t/I_y{}^1I_y{}^2$
q_2 = $I_y{}^2/I_y$
q_1 = $I_y{}^1/I_y$
r_x, r_y, w = coordinates of control mass m_c in x, y, z coordinate system
u = control force
v = $\dot{w}$
w = displacement of the control mass m_c (see Fig. 2)
$\alpha(0)$ = $I_{yz}(0)/(I_z-I_y)$
$\beta(0)$ = $-I_{xz}(0)/(I_z-I_x)$
ζ_i = damping factor for the ith mode due to feedback control
γ = p_3/p_1
Ω_x, Ω_y = transverse angular velocity components of the crew quarters
$\bar{\Omega}$ = nominal space station spin velocity
λ = θ
θ = torsional rotation of body 2 relative to body 1

Received June 6, 1973; revision received October 10, 1973. The work reported here was supported by NASA Contract NAS8-27952, and administered by the Marshall Space Flight Center, Alabama. This support is gratefully acknowledged.

Index categories: Space Station Systems, Manned; Spacecraft Attitude Dynamics and Control.

* Associate Professor of Mechanical Engineering and Engineering Management. Member AIAA.

† Research Assistant, Mechanical Engineering Department.

Introduction

A SPACECRAFT is said to be "wobbling" when its axis of maximum moment of inertia is not aligned with its moment-of-momentum vector. This undesirable vehicle motion can be controlled by the use of reaction jets, passive dampers, control moment gyros (CMG's) and momentum wheels. Each of these devices has both advantages and disadvantages, and Dr. Eugene Worley (Marshall Space Flight Center, S & E-AERO-R) suggested in the summer of 1970 the possibility of an active system which would employ a single movable mass to generate control torques. The stimulus for this proposition was the observation that astronaut motion within the space station (moving masses) would be the principal source of spacecraft wobble motion. It therefore seemed reasonable to assume that controlled motion of a comparable mass could be used to eliminate wobble motion. Reference 1 demonstrates that a movable mass controller (MMC) represents an extremely attractive alternative for the wobble damping of spacecraft which basically behave like a rigid body. The present study was designed to establish the feasibility of an MMC in the attitude stabilization of a cable-connected artificial-g configuration which cannot reasonably be idealized as a rigid body.

Dynamic Models

Introduction

Most of the past analyses of cable-connected rotating space station configurations have been concerned with a) the dynamic

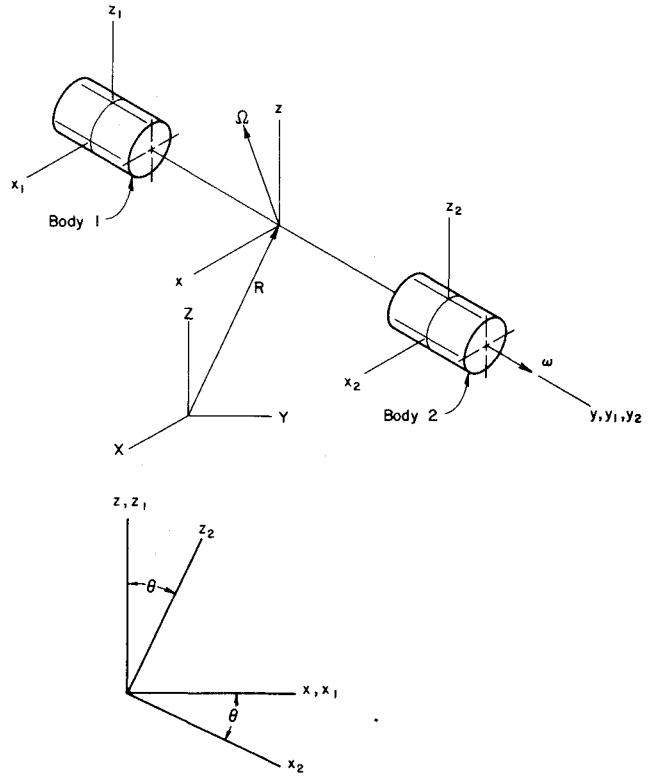

Fig. 1 Basic kinematic definitions.

formulation of the problem, or b) the stability of the system. Typical dynamic formulations have considered the extensional motion of the system[2,3] or have considered lateral motion of the cables[4,5] with the end bodies assumed to be particles. Stabekis and Bainum[6] have also examined the problem with an extensible cable but consider the end masses to be rigid bodies. Nixon[7] has recently presented a reasonably general linearized formulation for a space station consisting of two rigid bodies connected by n elastic cables.

The general motion of a space station can be conveniently described via Likin's[8] formulation which employs a body-fixed coordinate system whose origin coincides with the space-station mass center. The elastic response of the space station relative to this coordinate system is then defined by "free-free" modal coordinates. These modes are lightly coupled via gyroscopic terms, and for the configuration illustrated in Fig. 1 consist of the following: a) a "torsional mode" about the y axis, b) two "bending" modes for pitch motion in the z-y plane, c) two "bending" modes for yaw motion in the x-y plane, and d) an extensional mode for relative motion along the y axis. For the type of configuration examined here, the following physical observations are valid: a) The natural frequency associated with the extensional mode is an order of magnitude higher than any other natural frequency, and this mode is not readily excited by particle mass motion within the space station. b) The natural frequencies of the bending modes (yaw and pitch) are an order of magnitude higher than either the "rigid-body" wobble frequency or the torsional natural frequency. c) To a first order (linear) approximation yaw motion is not affected by either astronaut or control mass motion. d) The torsional natural frequency is of the same order of magnitude as the "rigid-body" wobble frequency.

The model derived in this study is intentionally simplified, and includes only the aggregate motion of the space station as a rigid body, and the relative "torsional" rotation of the counterweight and crew quarters. The simplicity of the model is a significant aid in understanding the dynamics of the controlled system.

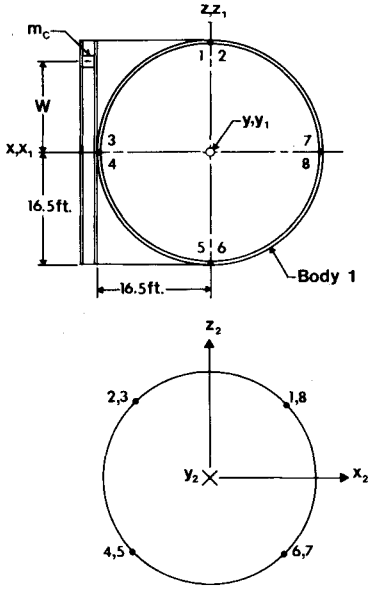

Fig. 2 The MMC configuration, and the McDonnell-Douglas cable configuration.

Governing Equations

Figures 1 and 2 illustrate the basic kinematic variables required to define the problem. The X, Y, Z axes of Fig. 1 define an inertial coordinate system. The x_1, y_1, z_1 and x_2, y_2, z_2 axes are fixed in rigid bodies 1 and 2, respectively, and their origins coincide with the mass centers of these bodies. Figure 2 illustrates the MMC system. The essential element of the stabilizer is the point mass m_c whose motion is limited by a tube (or other physical constraints) to be parallel with the z_1 axis. The tube is attached to body 1, and the position of the mass within the tube is defined by the variable w. The x, y, z axes of Fig. 1 are parallel, respectively, to the x_1, y_1, z_1 axes, and the origin of the x, y, z system coincides with the net mass center of the system (body 1, body 2, and the nominal position of the point mass m_c). The position of the control mass in the x, y, z system is defined by the vector $\mathbf{r} = \mathbf{i}r_x + \mathbf{j}r_y + \mathbf{k}w$, and its nominal position is defined by the vector $\tilde{\mathbf{r}} = \mathbf{i}r_x + \mathbf{j}r_y$. The x_2, y_2, z_2 axes of Fig. 1 are principal axes for body 2. The angle θ defined the (only) relative motion between the x, y, z (x_1, y_1, z_1) axes and the x_2, y_2, z_2 axes. The vector $\mathbf{R}$ locates the origin of the x, y, z system in the X, Y, Z system. The angular velocity of the x, y, z system relative to the X, Y, Z system is defined by the vector $\boldsymbol{\Omega}$, and the angular velocity of the x_2, y_2, z_2 system relative to the x, y, z system is defined by the vector $\boldsymbol{\omega}$.

Body 1 of Fig. 1 corresponds to the crew quarters, while body 2 corresponds to the counterweight. By spinning the system about a transverse axis of maximum moment of inertia (nominally the z axis) an artificial-g environment is induced in the crew quarters.

The vectors $\boldsymbol{\rho}^1$ and $\boldsymbol{\rho}^2$ denote the position vectors in the x_1, y_1, z_1 and the x_2, y_2, z_2 systems, and the vectors $\mathbf{a}^1$ and $\mathbf{a}^2$ locate the origins of the x_1, y_1, z_1 and x_2, y_2, z_2 systems in the x, y, z system. Hence, by definition

$$\int_{m_1} \boldsymbol{\rho}^1\, dm = 0, \quad \int_{m_2} \boldsymbol{\rho}^2\, dm = 0, \quad m_1\mathbf{a}^1 + m_2\mathbf{a}^2 + m_c\tilde{\mathbf{r}} = 0 \tag{1}$$

where m_1 and m_2 are the masses of bodies 1 and 2, respectively.

The following two derivative operations with respect to time are required

$$\dot{\mathbf{V}} = \left.\frac{dV}{dt}\right|_{X,Y,Z}, \qquad \hat{\mathbf{V}} = \left.\frac{dV}{dt}\right|_{x,y,z}$$

where **V** is an arbitrary vector. The following notation will be used to identify the coordinate system in which the component description of a vector is stated: (V) implies a component description in the x, y, z or x_1, y_1, z_1 system, while $(V)_{i2}$ implies a component description in the x_2, y_2, z_2 system. These vectors are related by the coordinate transformation

$$(V)_{i2} = [\theta](V) = \begin{bmatrix} c\theta & 0 & -s\theta \\ 0 & 1 & 0 \\ s\theta & 0 & c\theta \end{bmatrix} (V) \tag{2}$$

where $s\theta \equiv \sin\theta$, and $c\theta \equiv \cos\theta$.

The first governing equation is the system moment-of-momentum equation defined by

$$\mathbf{T}^r = \int_{m_1} (\mathbf{a}^1 + \boldsymbol{\rho}^1) \times (\ddot{\mathbf{R}} + \ddot{\mathbf{a}}^1 + \ddot{\boldsymbol{\rho}}) \, dm + \int_{m_2} (\mathbf{a}^2 + \boldsymbol{\rho}^2) \times (\ddot{\mathbf{R}} + \ddot{\mathbf{a}}^2 + \ddot{\boldsymbol{\rho}}^2) \, dm + m_c \mathbf{r} \times (\ddot{\mathbf{R}} + \ddot{\mathbf{r}}) \tag{3}$$

where T^r is the resultant external torque applied to the system at the origin of the x, y, z system. From Eq. (1) and the kinematic results

$$\begin{aligned} \ddot{\mathbf{a}}^i &= \dot{\boldsymbol{\Omega}} \times \mathbf{a}^i + \boldsymbol{\Omega} \times (\boldsymbol{\Omega} \times \mathbf{a}^i); \quad i = 1, 2 \\ \ddot{\mathbf{r}} &= \hat{\ddot{\mathbf{r}}} + 2\boldsymbol{\Omega} \times \hat{\dot{\mathbf{r}}} + \dot{\boldsymbol{\Omega}} \times \mathbf{r} + \boldsymbol{\Omega} \times (\boldsymbol{\Omega} \times \mathbf{r}) \\ \ddot{\boldsymbol{\rho}}^1 &= (\dot{\boldsymbol{\Omega}} \times \boldsymbol{\rho}^1) + \boldsymbol{\Omega} \times (\boldsymbol{\Omega} \times \boldsymbol{\rho}^1) \\ \ddot{\boldsymbol{\rho}}^2 &= (\dot{\boldsymbol{\Omega}} \times \boldsymbol{\rho}^2) + [(\hat{\dot{\omega}}) + (\boldsymbol{\Omega} \times \boldsymbol{\omega})] \times \boldsymbol{\rho}^2 + (\boldsymbol{\Omega} + \boldsymbol{\omega}) \times [(\boldsymbol{\Omega} + \boldsymbol{\omega}) \times \boldsymbol{\rho}^2] \end{aligned} \tag{4}$$

one obtains for Eq. (3)

$$(T^r) = [J](\dot{\Omega}) + [(\Omega)][J](\Omega) + [J^2](\hat{\dot{\omega}}) + [(\omega)][J^2](\omega) + [(d)](\omega) + m_c[(r)](\hat{\ddot{r}}) + 2m_c[(r)][(r)](\hat{\dot{r}}) \tag{5}$$

where $[J]$ is the system moment of inertia defined by

$$[J] = [J^1] + [J^2] - \sum_{i=1}^{2} \{m_i[(a^i)][(a^i)] + m_c[(r)][(r)]\} \tag{6}$$

and $[J^1]$ and $[J^2]$ are the inertia matrices for bodies 1 and 2 (relative to their individual mass centers), in the x, y, z system. The matrix $[J^2]$ is further defined by

$$[J^2] = [\theta]^T [J_{i2}{}^2][\theta] \tag{7}$$

where $[J_{i2}{}^2]$ is the inertia matrix of body 2 in terms of the x_2, y_2, z_2 system. In Eq. (5), the notation $[(\,)]$ implies

$$[(V)] = \begin{bmatrix} 0 & -V_z & V_y \\ V_z & 0 & -V_x \\ -V_y & V_x & 0 \end{bmatrix} \tag{8}$$

and performs the matrix equivalent of the vector cross-product operation, i.e., $(A \times B) = [(A)](B)$. Returning to Eq. (5), the vector (d) is defined by

$$(d) = \{j[U] - 2[J^2]\}(\Omega), \qquad j = \text{trace}\,[J^2]. \tag{9}$$

where $[U]$ is the unity matrix.

The fact that $\ddot{\mathbf{R}}$ is present in Eq. (3) and absent in Eq. (5) is primarily explained by the assumption that the space station is in a circular orbit. Because of Eq. (1), the absent coupling term in Eq. (5) is $m_c(\mathbf{k}w \times \ddot{\mathbf{R}})$, which is demonstrably[1] negligible.

The definition of the vectors $\boldsymbol{\Omega}$ and $\boldsymbol{\omega}$ is completed by the independent equation

$$\mathbf{T}^c = \int_{m_2} \boldsymbol{\rho}^2 \times (\ddot{\mathbf{R}} + \ddot{\mathbf{a}}^2 + \ddot{\boldsymbol{\rho}}^2) \, dm \tag{10}$$

where $\mathbf{T}^c$ is the resultant torque applied to body 2 at its mass center. Substituting from Eqs. (1) and (4) into Eq. (10) yields

$$(T^c)_{i_2} = [J_{i_2}{}^2](\dot{\Omega})_{i_2} + [(\Omega)_{i_2}][J_{i_2}{}^2](\Omega)_{i_2} + [J_{i_2}{}^2](\hat{\dot{\omega}})_{i_2} + [(\omega)_{i_2}][J_{i_2}{}^2](\omega)_{i_2} + [(d)_{i_2}](\omega)_{i_2} \tag{11}$$

Since the x_2, y_2, z_2 axes are principal axes for body 2, the y component of Eq. (11) yields

$$T_y^c = I_y{}^2\dot{\Omega}_y + I_y{}^2\ddot{\theta} + (I_{z_2}{}^2 - I_{x_2}{}^2)\{(\Omega_z{}^2 - \Omega_x{}^2)s\theta c\theta - \Omega_x\Omega_z c(2\theta)\} \tag{12}$$

where $I_{x_2}{}^2, I_{y_2}{}^2, I_{z_2}{}^2$ are the moments of inertia for body 2 relative to the x_2, y_2, z_2 principal axes, respectively. The assumption is made in this study that T_y^c is the reaction torque defined by

$$T_y^c = -k_t\theta \tag{13}$$

where k_t is a torsional spring constant.

The governing equation of motion for w is[3]

$$f_z = m_c\{\ddot{w} + (\dot{\Omega}_x r_y - \dot{\Omega}_y r_x) + r_x\Omega_z\Omega_x + r_y\Omega_z\Omega_y - w(\Omega_x{}^2 + \Omega_y{}^2)\} \tag{14}$$

where f_z is the z component of the reaction force applied to m_c.

Summarizing, the state variables $(\Omega_x, \Omega_y, \Omega_z, \theta, w)$ are defined by Eqs. (5, 12, and 14). From Eq. (6), the inertia matrix $[J]$ is seen to be a function of both w and θ. Of particular importance are the relationships

$$\begin{aligned} I_{xz} &= I_{xz}(0) + m_c r_x w - (I_{z_2}{}^2 - I_{x_2}{}^2)s\theta c\theta \\ I_{yz} &= I_{yz}(0) + m_c r_y w \end{aligned} \tag{15}$$

Uncontrolled Motion : Linearized Model

The free motion dynamics problem can be summarized as follows. Under ideal conditions, the H (moment-of-momentum) vector and the axis of maximum moment of inertia of the space station coincide. If (due to either external torques or internal mass motion) the two are forced apart, a condition generally called "wobbling" results. This motion is characterized by a nominally constant rotation rate about the z axis accompanied by oscillations in Ω_x, Ω_y, and θ.

The defining equations for free motion are obtained from Eqs. (5) for $r = 0$, and Eq. (12), and a valid linearization of these equations is possible based on the following observations: a) $\Omega_z \simeq \bar{\Omega}$, the average spin velocity, b) Ω_x and Ω_y are very small in comparison to $\bar{\Omega}$, and c) θ is generally small justifying the approximations $c\theta \cong 1$, $s\theta \cong \theta$.

The resultant linearized equations are

$$\begin{aligned} \dot{\Omega}_x &= -\Omega_y a\bar{\Omega} + \theta e(1 - b_2)\bar{\Omega} - a\bar{\Omega}^2\alpha(0) \\ \dot{\Omega}_y &= \Omega_x b_1\bar{\Omega} + (k_t/I_y{}^1)\theta - b\bar{\Omega}^2\beta(0)/q_1 \\ \ddot{\theta} &= -\Omega_x(b - b_2)\bar{\Omega}/q_1 - (P^2 + b_2\bar{\Omega}^2)\theta + b\bar{\Omega}^2\beta(0)/q_1 \end{aligned} \tag{16}$$

where the result, $b_1 = (b - q_2b_2)/q_1$, is employed. Two special cases can be obtained from these equations. First, if $k_t \to \infty$, the rigid body equations result.

$$\begin{aligned} \dot{\Omega}_x &= -\Omega_y a\bar{\Omega} - a\bar{\Omega}^2\alpha(0) \\ \dot{\Omega}_y &= \Omega_x b\bar{\Omega} - b\bar{\Omega}^2\beta(0) \end{aligned} \tag{17}$$

with the rigid-body wobble frequency

$$p_1 = \bar{\Omega}(ab)^{1/2} \tag{18}$$

Equation (17) may be obtained from Eq. (16) by using Laplace transforms to eliminate θ, and performing the limit $k_t \to \infty$. The second special case results if $k_t = 0$. Since $e = I_y{}^2/I_x$ is in general quite small, the resultant motion is approximately defined by

$$\begin{aligned} \dot{\Omega}_x &= -\Omega_y a\bar{\Omega} - a\bar{\Omega}^2\alpha(0) \\ \dot{\Omega}_y &= \Omega_x b_1\bar{\Omega} - b\bar{\Omega}^2\beta(0)/q_1 \\ \ddot{\theta} &= -\Omega_x(b - b_2)\bar{\Omega}/q_1 - b_2\bar{\Omega}^2\theta + b\bar{\Omega}^2\beta(0)/q_1 \end{aligned} \tag{19}$$

The crew quarters wobble frequency and the torsional oscillation frequency p_2 are defined by

$$p_1 = \bar{\Omega}(ab_1)^{1/2}, \qquad p_2 = \bar{\Omega}b_2{}^{1/2} \tag{20}$$

Controlled Motion : Linearized Model

As stated previously, motion of the complete system is defined by Eqs. (5, 12, and 14). A valid linearization of the controlled system is possible based on the preceding assumptions for free motion ($\Omega_z \cong \bar{\Omega}$; $\Omega_x, \Omega_y \ll \bar{\Omega}$; $s\theta \cong \theta$, $c\theta \cong 1$) plus the following assumptions for the MMC: a) $m_c w^2/I_x \ll 1$, $m_c w^2/I_y \ll 1$, and b) the "coriolis-torques" $2m_c w\dot{w}\Omega_x$ and $2m_c w\dot{w}\Omega_y$ which arise in Eq. (14) due to the term $2m_c[(r)][(\Omega)](\hat{\dot{r}})$ are negligible.

The resultant linearized equations may be written as

$$\begin{Bmatrix} \dot{\Omega}_x \\ \dot{\Omega}_y \\ \dot{\lambda} \\ \dot{\theta} \\ \dot{v} \\ \dot{w} \end{Bmatrix} = \begin{bmatrix} 0 & -\bar{\Omega}a & \bar{\Omega}e(1-b_2) & 0 & 0 & -\bar{\Omega}^2 g_2 \\ \bar{\Omega}b_1 & 0 & 0 & k_t/I_y{}^1 & 0 & \bar{\Omega}^2 g_1 \\ -\bar{\Omega}(b-b_2)/q_1 & 0 & 0 & -(b_2\bar{\Omega}^2+P^2) & 0 & -\bar{\Omega}^2 g_1 \\ 0 & 0 & 1 & 0 & 0 & 0 \\ \bar{\Omega}r_x(b_1-1) & \bar{\Omega}r_y(a-1) & -\bar{\Omega}r_y e(1-b_2) & r_x k_t/I_y{}^1 & 0 & \bar{\Omega}^2 e_1 \\ 0 & 0 & 0 & 0 & 1 & 0 \end{bmatrix} \begin{Bmatrix} \Omega_x \\ \Omega_y \\ \lambda \\ \theta \\ v \\ w \end{Bmatrix} + \begin{Bmatrix} -r_y/I_x \\ r_x/I_y{}^1 \\ -r_x/I_y{}^1 \\ 0 \\ (1+e_1)/m_c \\ 0 \end{Bmatrix} u + \bar{\Omega}^2 \begin{Bmatrix} -a\alpha(0) \\ -b\beta(0)/q_1 \\ b\beta(0)/q_1 \\ 0 \\ r_y a\alpha(0) - r_x b\beta(0)/q_1 \\ 0 \end{Bmatrix} \tag{21}$$

In the equation above, u is the control contribution to the force f_z appearing in Eq. (14). A comparison between the solutions from this linear model with those of the general nonlinear model [Eqs. (5, 12, and 14)] for a wide range of cases revealed no significant differences. In most cases no discernible differences were evident in plots of the solutions.

Data, Agreements, and Assumptions

Control Objectives and Constraints

The general attitude-stabilization control objective may be defined in terms of the control force u and the state-variable vector X (Ω_x, Ω_y, λ, θ, v, w). In terms of these variables, the basic requirement is the synthesis of a feedback control logic $u = u(X)$ which satisfies the following descending order of objectives:

a) The attitude-stabilization system is required to eliminate the oscillations in the transverse angular velocity components of body 1 (Ω_x, Ω_y), i.e., the desired terminal state is $\Omega_x(t_f) = \Omega_y(t_f) = 0$.

b) While the comfort of the astronauts does not explicitly depend on θ also being forced to zero, for $k_t > 0$ the coupling of the system is such that condition (a) cannot generally be otherwise satisfied. Hence, an additional desired terminal state is $\theta(t_f) = 0$.

c) The full capacity of the controller should be restored after a disturbance has been eliminated, hence, the additional desired terminal state $w(t_f) = \dot{w}(t_f) = 0$.

In summary, the desired terminal state is

$$\Omega_x(t_f) = \Omega_y(t_f) = \theta(t_f) = w(t_f) = \dot{w}(t_f) = 0 \tag{22}$$

The basic constraint on the controller's performance is the physical limitation on the magnitude of w, i.e.,

$$|w| \leqq W = 16.5 \text{ ft} \tag{23}$$

In addition to this specific constraint, control laws were sought which generally minimized the peak control force magnitude $|u|_{\max}$. To achieve simplicity, a control law of the form

$$u = k_1\Omega_x + k_2\Omega_y + k_3\dot{\theta} + k_4\theta + k_5\dot{w} + k_6 w + k_7 \int_0^t w(\tau)\, d\tau \tag{24}$$

was employed. The integral term in this equation was added to enforce the terminal boundary condition $w(t_f) = 0$.

In general terms, the control synthesis problem addressed here can be stated as follows. Determine those gains k_i which will cause the controlled system to rapidly recover from an initial disturbance, and to approach the desired terminal state given in Eq. (22) without violating the constraint of Eq. (23). In addition, minimization of the peak control force $|u|_{\max}$ is desired.

Table 1 Axial space-station dimensions

Deployment stage	C_1	C_2	Cable length	r_y
0	57.16	166.2	0.0	−51.5
$\frac{1}{4}$	69.28	201.4	35.3	−63.6
$\frac{1}{2}$	81.41	236.7	70.5	−75.8
$\frac{3}{4}$	93.53	272.0	105.8	−87.9
1	105.7	307.2	141.0	−100.0

Space-Station Configurations and Data

The space-station configuration examined in this study is based on a McDonnell-Douglas[9] astronautics proposed design. Table 1 illustrates the significant longitudinal dimensions of this space-station design in its various stages of deployment. The parameters C_1 and C_2 of this table are the distance from the center of mass of body 1 to the system mass center and the mass center of body 2, respectively. The inertial properties of the space-station are provided in Table 2.

Reference Disturbance and Controller Sizing

The reference disturbance used throughout this study consists of four astronauts (773 lb or 24 slugs) moved instantaneously to the worst [maximum $I_{xz}(0)$ and $I_{yz}(0)$] possible locations within the crew quarters. The resultant initial product-of-inertia disturbances for the fully deployed configuration are

$$I_{xz}(0) = 3250 \text{ slug-ft}^2, \quad I_{yz}(0) = 51{,}000 \text{ slug-ft}^2 \tag{25}$$

These product-of-inertia were used for all stages of deployment.

Equation (15) demonstrates the linear dependence of the I_{xz} and I_{yz} product of inertias upon the controller position w, and it is primarily through this dependence that the MMC system is used to generate control torques. The MMC considered in this study is defined by the parameters

$$r_x = 16.5 \text{ ft}, \qquad m_c = 11 \text{ slugs} \tag{26}$$

The parameter r_y depends upon the stage of deployment and is defined in Table 1. The product-of-inertia capacity of the controller is from Eqs. (15) and (26) $I_{xz}{}^c = 3000$ slug-ft^2, $I_{yz}{}^c = 18{,}200$ slug-ft^2 ($r_y = 100$ ft). The equivalent static torque capability (for $\bar{\Omega} = 4$ rpm, and $r_y = 100$ ft) is approximately $|T_x|_{\max} = |I_{yz}{}^c|\bar{\Omega}^2 = 3180$ ft-lbs, and $|T_y|_{\max} = |I_{xz}{}^c|\bar{\Omega}^2 = 525$ ft-lbs. Since the product of inertias are linear functions of w, the control torques may be varied linearly from zero to full capacity.

Deployment and Retraction Procedures

The assumption was made in this study that the deployment procedure would be initiated by overspinning the rigidly assembled space-station prior to deployment. As deployment proceeds, the spin moment of inertia I_z increases and the spin velocity drops. When fully deployed, the space station rotates at 4 rpm. This deployment procedure yields spin rates of 11.5, 8.30, 6.28, and 4.85 rpm for the 0, $\frac{1}{4}$, $\frac{1}{2}$, and $\frac{3}{4}$ stages of deployment, respectively.

Table 2 Inertia properties and parameters[a]

Deployment stage	I_x (slug-ft^2)	I_z (slug-ft^2)	a
0	64.926×10^6	65.009×10^6	0.9796
$\frac{1}{4}$	90.166×10^6	90.249×10^6	0.9853
$\frac{1}{2}$	119.91×10^6	119.99×10^6	0.9889
$\frac{3}{4}$	154.13×10^6	154.21×10^6	0.9914
1	187.10×10^6	187.18×10^6	0.9929

[a] Constant inertia parameters: $I_y{}^1 = 0.621^6 \times 10^6$ slug-ft^2, $I_y{}^2 = 0.787 \times 10^6$ slug-ft^2, $I_y = 1.407 \times 10^6$ slug-ft^2, and $b_2 = 0.0500$, $b_1 = 0.0709$, $b = 0.0592$.

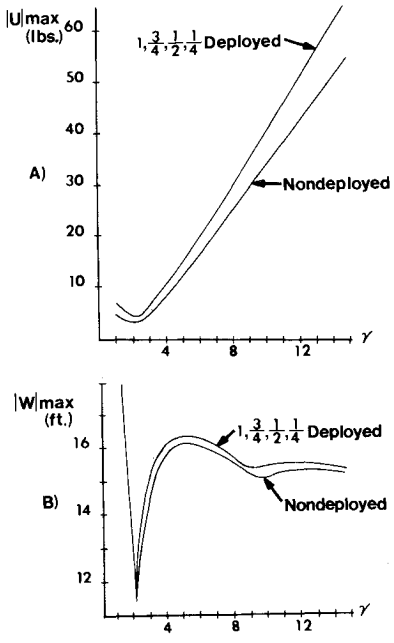

Fig. 3 a) $|u|_{max}$ vs $\gamma = p_3/p_1$, and b) $|w|_{max}$ vs γ.

Torsional Stiffness Coefficients

The two following configurations were used in defining the torsional stiffness k_t: a) a zero torsional stiffness configuration ($k_t = 0$), corresponding to a single cable design, and b) a high torsional stiffness configuration corresponding to the McDonnell-Douglas design.

The McDonnell-Douglas configuration employs eight cables in the "basket-weave" pattern illustrated in Fig. 2. The numbers in Fig. 3 correspond to cable attachment points. The torsional stiffness of this arrangement depends on the load carried in the cable and the cylindrical radius of the two bodies. Calculation of the torsional stiffness coefficient k_t for this design was based on an analysis by Nixon.[7] By neglecting the "stretch" of the cables, the governing equation is

$$k_t = F_c(16.5)^2/8l_o(2)^{1/2}$$

where F_c is the resultant centrifugal force acting on all of the cables, and l_o is the total deployed cable length. The numerical constants in this equation arise from the geometry of Fig. 2. The calculated values for torsional stiffness k_t are summarized below in Table 3.

Synthesis Procedure

From Eqs. (21) and (23), the dynamic system has the form

$$\dot{X} = AX + bu + f, \qquad u = k^T x \tag{27}$$

or in closed-loop form

$$\dot{X} = [A + bk^T]X + f \tag{28}$$

Table 3 Calculated torsional stiffness definitions

Stage	(rpm)	k_t (ft-lb/rad)
1/4	4	3.386×10^5
	8.3	1.650×10^6
1/2	4	2.254×10^5
	6.52	5.480×10^5
3/4	4	1.726×10^5
	4.85	2.544×10^5
1	4	1.463×10^5

Since the system is (in general) completely controllable, gains k_i can be determined which will yield any specified pole location for the closed-loop transfer function. The pole-specification approach was the basic synthesis tool employed in this study.

The general procedure for selecting desired root locations can be explained as follows. First, one notes from Eq. (21), that without control the mass motion is itself unstable due to the coefficient $A_{56} = \bar{\Omega}^2 e$. Assuming that the controller is stabilized (via the $k_6 w$ term in Eq. (24) with all other $k_i = 0$), the system defined by Eq. (21) has the following three undamped and largely uncoupled modes of motion: a) wobble motion involving Ω_x and Ω_y (natural frequency $= p_1$), b) torsional motion involving λ and θ (natural frequency $= p_2$), and c) control mass motion involving v and w (natural frequency $= p_3$). Hence, the characteristic equation for the uncontrolled system has the form

$$\prod_{i=1}^{3} (s^2 + p_i^2) = 0 \tag{29}$$

The gains k_i are to be selected so that the closed-loop characteristic equation has the form

$$(s + p_0) \prod_{i=1}^{3} (s^2 + 2\zeta_i p_i s + p_i^2) = 0 \tag{30}$$

where the $(s + p_0)$ term arises due to the integral feedback term.

An examination of this transfer function reveals that root specification entails selecting the following parameters: a) ζ_i; $i = 1, 2, 3$, b) p_3, the natural frequency of the control mass, and c) p_0, the pole location due to the integral feedback term. In short, the control synthesis problem entails choosing these five (independent) parameters in some fashion that will yield the desired transient behavior of the controlled system. A direct attack on this problem via a trial-and-error approach would be both laborious and time consuming, since there are five parameters to be varied. Furthermore, the quality of performance for each choice of parameters must be checked by generating a transient solution for the complete closed-loop system.

Accordingly, the following set of rules were established to reduce the magnitude of the control synthesis problem:

a) The damping factor for the wobble motion root was prescribed to be unity, i.e., $(s^2 + 2\zeta_1 p_1 s + p_1^2) = (s + p_1)^2$.
b) The damping factors for the control mass and torsional motion were selected to yield damping constants equivalent to that obtained for wobble motion, i.e., $\zeta_1 p_1 = \zeta_2 p_2 = \zeta_3 p_3$.
c) The pole p_0 was chosen to enforce the control mass final position $w(t_f) = 0$, without significantly influencing the initial dynamics of the system. The value for p_0 was chosen such that $\exp(-p_0 t) = 0.10$ at $t = 80$ sec; hence $p_0 = 0.2878$ sec^{-1} for all cases.

Rule (a) is enforced to meet the priority control objective, viz., optimum wobble damping rates, and rule (b) causes a uniform (in time) attenuation of all system modes. By this somewhat arbitrary procedure, the synthesis problem is reduced to the determination of a suitable value for the control mass natural frequency p_3. The dependence of system performance upon p_3 is established (for each configuration) by the following steps:

a) A value for the root p_3 is selected, and the uncontrolled system natural frequencies p_1, p_2 are calculated. These values together with the rules cited above, define the closed-loop system poles.
b) Gains k_i are determined which yields the specified closed-loop poles.
c) A transient solution for the closed-loop system is generated to determine $|u|_{max}$ and $|w|_{max}$, and to establish the "quality" of control.

Results

Introduction

The results presented here demonstrate the influence of the following factors on controller performance: a) stage of deployment, b) nominal spin velocity $\bar{\Omega}$, and c) torsional stiffness k_t.

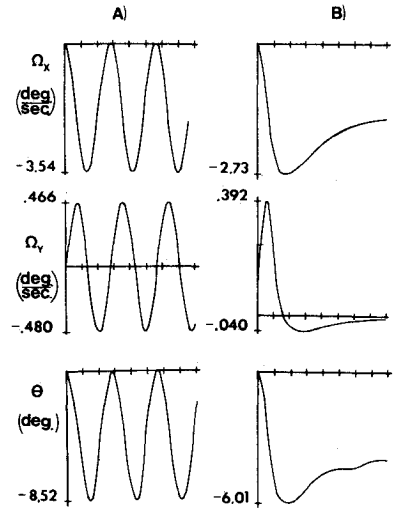

Fig. 4 Uncontrolled (a) and controlled (b) system transient response for the fully deployed system; $\bar{\Omega} = 4$ rpm, and $k_t = 0$. Each time division equals 20 sec.

The principal criteria for evaluating controller performance are the peak transient values of u and w ($|u|_{max}$ and $|w|_{max}$) that result from the standard disturbance of Eq. (25). The dimensionless parameter $\gamma = p_3/p_1$ has proven helpful in summarizing the results.

Undeployed and Zero Torsional Stiffness Cases

Figure 3 illustrates the transient performance of the closed-loop system for the non-deployed configuration, and the deployed configurations with $k_t = 0$. The values of $|w|_{max}$ and $|u|_{max}$ illustrated in this figure were obtained from transient solution of the closed-loop system. In particular, the closed-loop system was given an initial disturbance (with zero initial conditions) defined by the product-of-inertias of Eq. (25). Because of the synthesis procedure employed, all cases illustrated are equivalent in the frequency domain, i.e., in all cases, crew quarter's wobble motion is critically damped, and $\zeta_3 p_3 = \zeta_2 p_2$. However, the gains associated with each point are generally different.

In the undeployed configuration, the space-station is a rigid body and no relative rotation between the crew quarters and counterweight exists. In the deployed $k_t = 0$ cases, the relative rotation is physically uncontrollable; however, since $k_t \doteq 0$, no disturbance is imparted to the crew quarters because of θ. Hence, control of θ was not a consideration in obtaining the results of Fig. 3.

The dependence of $|u|_{max}$ on γ for $\bar{\Omega} = 4$ rpm is illustrated in Fig. 3a. The results for $|u|_{max}$ for the overspin cases showed a direct proportionality to the spin-velocity squared $\bar{\Omega}^2$, and the over-spin results may be calculated directly from Fig. 3a. The results of this figure support the following additional conclusions: a) for constant spin velocity, and constant γ, $|u|_{max}$ is virtually independent of the stage of deployment, and b) for a given spin velocity and deployment stage, $|u|_{max}$ is an approximately linear function of γ. Further, $|u|_{max}$ has a minimum with respect to γ at approximately $\gamma = 2$.

The dependence of $|w|_{max}$ on the variables γ, $\bar{\Omega}$, and the stage of deployment is illustrated in Fig. 3b. Within the range of spin velocity investigated the results were independent of $\bar{\Omega}$, and an inspection of Fig. 3b confirms the comparative independence of the results on the stage of deployment. However, the dependence of $|w|_{max}$ on γ is seen to be dramatic with a minimum occurring at approximately $\gamma = 2$. The minimum point is characterized by $w_{min} = -|w|_{max}$, $w_{max} = |w|_{max}$, i.e., the variations in w both above and below zero are equal. For the disturbance employed in this study, the maximum amplitudes to the right and left of this point were, respectively, positive and negative. Obviously, these signs depend on the sign of the disturbance. On the basis of the results presented in Fig. 3, the "best" range of γ for the configurations considered would be between 2 and 3. This range for γ yields approximate minima for both $|u|_{max}$ and $|w|_{max}$.

The fact that $|w|_{max}$ is largely independent of $\bar{\Omega}$, while $|u|_{max}$ is proportional to $\bar{\Omega}^2$ is easily explained by an inspection of Eqs. (15) and (21). From Eq. (21), the disturbance torques due to the initial product of inertias are proportional to $\bar{\Omega}^2$. Hence, the required control torques should also be proportional to $\bar{\Omega}^2$, which explains the increase in $|u|_{max}$. However, the control torques generated by w arise through the linear dependence of the product of inertias in Eq. (15) on w. Hence, the peak control torques which are generated by w motion will be proportional to $\bar{\Omega}^2$, and a change in $|w|_{max}$ is not required for increasing $\bar{\Omega}$.

The fact that both $|u|_{max}$ and $|w|_{max}$ are unaffected by variations in the deployment stages $(1, \frac{3}{4}, \frac{1}{2}, \frac{1}{4})$ is explained by an inspection of Tables 1 and 2 and Eq. (21). For $k_t = 0$, the only parameters which vary with the stage of deployment are r_y and a. From Table 2, the variations in a over the deployment stages 1, $\frac{3}{4}$, $\frac{1}{2}$, $\frac{1}{4}$, is seen to be negligible. From Table 1, the variation in r_y over these deployment stages is significant; however, the terms in which r_y is a factor in Eq. (21) are all small, and a significant variation in these small terms has a negligible influence on systems dynamics. In particular, the comparative smallness of the terms e, g_2, $(a-1)$, r_y/I_x, and $\alpha(0)$ in Eq. (21) accounts for the independence of controller performance to variations in r_y over the deployment stages 1, $\frac{3}{4}$, $\frac{1}{2}$, $\frac{1}{4}$. Differences in the controller performance illustrated in Fig. 4 for the nondeployed and deployed configurations is accounted for by a discontinuous change from the two-body model of Eq. (21) to the rigid-body model of Eq. (17).

Figure 4 illustrates the transient behavior of the fully deployed configuration both with and without control. The transient performance of the controller is illustrated in Fig. 5a. The pertinent data for this case are provided in Table 4 below. The superior performance of the controller is evident in a comparison of the variables Ω_x, Ω_y in Fig. 4.

Table 4 The fully deployed configuration, $\bar{\Omega} = 4$ rpm, $k_t = 0$

Input data: $p_1 = 0.1111$ rad/sec, $p_2 = 0.093$ rad/sec, $p_3 = 0.244$ rad/sec, $\gamma = 2.2$
Control data: $\zeta_1 = 1.0$, $\zeta_2 = 0.0$, $\zeta_3 = 0.454$
$k_1 = -149.46$ lb sec/rad, $k_2 = -2722$ lb sec/rad
$k_3 = k_4 = 0$, $k_5 = -4.384$ lb sec/ft
$k_6 = -1.3617$ lb/ft, $k_7 = -0.01776$ lb/ft sec
Peak mechanical power consumption = 6 w

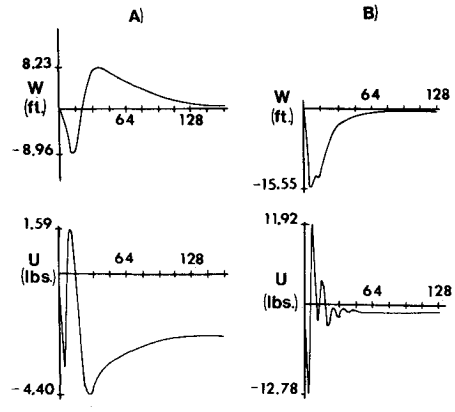

Fig. 5 Controller performance for a) $\bar{\Omega} = 4$ rpm, $k_t = 0$, and b) $\bar{\Omega} = 4$ rpm, $k_t = 1.463 \times 10^5$ ft lb/rad.

Table 5 The fully deployed configuration, $\bar{\Omega} = 4$ rpm, $k_t = 1.463 \times 10^5$ ft lb/rad

Input data: $p_1 = 0.1013$ rad/sec, $p_2 = 0.6574$ rad/sec, $p_3 = 0.2026$ rad/sec, $\gamma = 2.0$
Control data: $\zeta_1 = 1.0$, $\zeta_2 = 0.154$, $\zeta_3 = 0.50$
$k_1 = -193.63$ lb sec/rad, $k_2 = -3840$ lb sec/rad
$k_3 = 7784$ lb sec/rad, $k_4 = 5333$ lb/rad
$k_5 = -3.5846$ lb sec/ft, $k_6 = -0.47030$ lb/ft
$k_7 = -0.01252$ lb/ft sec
Peak mechanical power consumption = 37 w

Finite Torsional Stiffness Cases

The physical consequence of a finite torsional stiffness k_t is the coupling of crew quarters and counter-weight wobble motion. From a controls viewpoint, it becomes both necessary and feasible to control θ. The transient performance of the finite k_t cases are summarized in Fig. 6.

Figure 6a illustrates the dependence of $|u|_{max}$ on the stage of deployment and the dimensionless parameter γ at $\bar{\Omega} = 4$ rpm. For all deployment stages and spin speeds examined, $|u|_{max}$ showed a direct proportionality to $\bar{\Omega}^2$. The results of Fig. 6a support the following additional conclusions: a) For a fixed value of $\bar{\Omega}$ and stage of deployment, $|u|_{max}$ increases as γ increases. b) The dependence of $|u|_{max}$ on γ is strongly dependent on the stage of deployment.

Figure 6b illustrates the dependence of $|w|_{max}$ to both the stage of deployment and γ at $\bar{\Omega} = 4$ rpm. The curves of this figure display the same basic behavior as that shown in Fig. 3b for the $k_t = 0$ cases. However, the curves here show a marked dependence on the deployment stage. The results obtained for $|w|_{max}$ at higher values of $\bar{\Omega}$ were substantially the same as that illustrated in Fig. 6b. Increasing the spin velocity causes some changes in $|w|_{max}$ for values of γ below the sharp minima located at approximately $\gamma = 1.5$. However, the results to the right of this value are substantially unchanged by increasing $\bar{\Omega}$.

The results for the $k_t = 0$ cases of Fig. 3 and the $k_t > 0$ cases of Fig. 6 are similar in the following respects: a) $|u|_{max}$ is proportional to $\bar{\Omega}^2$, and b) $|w|_{max}$ is relatively independent of $\bar{\Omega}$. The explanation provided in the preceding section for these phenomena when $k_t = 0$ also holds for Fig. 6. The phenomenon of Fig. 6 which requires additional explanation is the marked dependence of system performance on the stage of deployment. As previously noted, variations in a and r_y which accompany changes in the stages of deployment have a negligible influence on system dynamics; however Table 3 shows that the torsional stiffness coefficient k_t varies markedly with the stage of deployment, and these changes in k_t account for the dependence of the results of Fig. 6 on the stage of deployment.

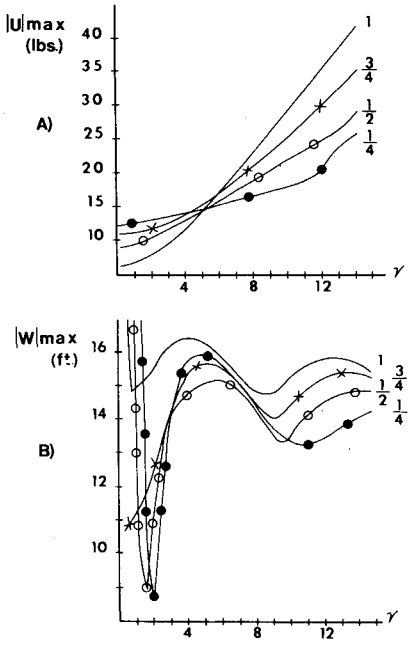

Fig. 6 a) $|u|_{max}$ vs $\gamma = p_3/p_1$, and b) $|w|_{max}$ vs γ.

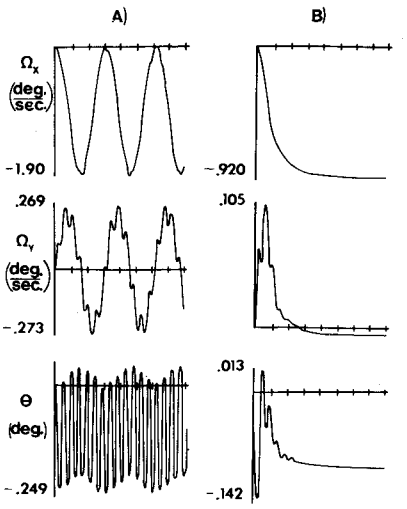

Fig. 7 Uncontrolled (a) and controlled (b) system transient response for the fully deployed system; $\bar{\Omega} = 4$ rpm, and $k_t = 1.463 \times 10^5$ ft lb/rad. Each time division equals 20 sec.

The solution curves of Fig. 6 for a transition from the fully deployed to the $\frac{1}{4}$ deployed configurations approach the non-deployed solution curve of Fig. 3. This result would be anticipated since as k_t increases, p_2 increases, and p_1 decreases approaching the rigid body wobble frequency $\bar{\Omega}(ab)^{1/2}$. In other words, a retraction deployment stage yields a continuous transition from the two-body model of Eq. (21) to the rigid-body model of Eq. (17).

Figure 7 illustrates the transient behavior of the fully deployed configuration both with and without control. The controller performance is illustrated in Fig. 5b. The pertinent data for this case are provided in Table 5. A comparison of the variables Ω_x, Ω_y, θ in Fig. 7 establishes the excellent performance of the controller. From Table 5, the value of γ for this case is seen to be 2.0. From Fig. 6, this value of γ yields near optimal performance. The choice of a best range for γ is seen to be largely dependent on the stage of deployment. For example, the best choice of γ for the $\frac{1}{4}$ deployment stage is near $\gamma = 2$, since this yields a minimum in both $|u|_{max}$ and $|w|_{max}$. However, for the fully deployed configuration, operating points near $\gamma = 1$ and $\gamma = 8$ are comparable in that both yield a minimum for $|w|_{max}$ with comparable requirements for $|u|_{max}$. A comparison of the controlled results in Fig. 5 ($k_t = 0$) and Fig. 7 ($k_t > 0$) demonstrates that the transient performance is better for $k_t > 0$, since no overshoot is present.

Conclusions

The MMC system discussed here provides a practical and attractive means for attitude-stabilization of the type of artificial-g space-stations examined here. The results presented demonstrate that the MMC can provide critical wobble damping rates for all stages of deployment, for extremes of spin velocity, and for two markedly different cable configurations. The results concerning the stage of deployment are of interest; however, since all stages of deployment must be experienced, they provide little insight into the proper design or operation of a space-station.

The results with respect to $\bar{\Omega}$ and k_t which bear on these points are as follows:

a) The peak control force $|u|_{max}$ is proportional to $\bar{\Omega}^2$; hence, control of the spin-velocity throughout deployment and retraction would markedly reduce the force requirements of the controller. In other words, overspin situations should be avoided.

b) The cable-configurations examined here are a single cable (zero torsional stiffness) design, and an eight cable (maximum torsional stiffness) design. In general, the single cable design is easier to control in the sense that smaller peak forces and control mass amplitudes are required. However, the control requirements for the MMC system are modest for both designs.

References

[1] Childs, D. W., "A Movable-Mass Attitude Stabilization System for Artificial-*g* Space Stations," *Journal of Spacecraft and Rockets*, Vol. 8, No. 8, Aug. 1971, pp. 829–834.

[2] Austin, F., "Nonlinear Dynamics of a Free-Rotating Flexibly Connected Double-Mass Space Station," *Journal of Spacecraft and Rockets*, Vol. 2, No. 6, Nov.–Dec. 1965, pp. 901–906.

[3] Crist, S. A. and Eisley, J. G., "Motion and Stability of a Spinning Spring-Mass System in Orbit," *Journal of Spacecraft and Rockets*, Vol. 6, No. 7, July 1969, pp. 819–824.

[4] Tai, C. L. and Loh, M. M. H., "Planar Motion of a Rotating Cable-Connected Space Station in Orbit," *Journal of Spacecraft and Rockets*, Vol. 2, No. 6, Nov.–Dec. 1965, pp. 889–894.

[5] Chobotov, V., "Gravity-Gradient Excitation of a Rotating Cable-Counterweight Space Station in Orbit," *Journal of Applied Mechanics*, Vol. 30, No. 4, Dec. 1963, pp. 547–554.

[6] Stabekis, P. and Bainum, P. M., "Motion and Stability of a Rotating Space Station-Cable-Counterweight Configuration," *Journal of Spacecraft and Rockets*, Vol. 7, No. 8, Aug. 1970, pp. 912–918.

[7] Nixon, D. D., "Dynamics of a Spinning Space Station with a Counterweight Connected by Multiple Cables," AIAA Paper 72-172, San Diego, Calif., 1972.

[8] Likins, P. W., "Modal Methods for Analysis of Free Rotations of Spacecraft," *AIAA Journal*, Vol. 5, No. 7, July 1967, pp. 1304–1309.

[9] McDonnell Douglas Astronautics Company-West, Space Station Definition, Vol. IV, Configuration Analysis Contract NAS8-25140, MSFC-DRL-160 Line Item 8, July 1970.